GEOPHYSICAL RESEARCH LETTERS, VOL. 25, NO. 12, PAGES 2213-2216, JUNE 15, 1998

Crustal structure of the flanks of the East Pacific Rise: Implications for overlapping spreading centers

Sara Bazin, Harm van Avendonk, Alistair J. Harding and John A. Orcutt

Cecil H. and Ida M. Green Institute of Geophysics and Planetary Physics, Scripps Institution of Oceanography, La Jolla.

J. Pablo Canales and Robert S. Detrick

Dept. of Geology and Geophysics, Woods Hole Oceanographic Institution, Woods Hole.

MELT group[1]

Abstract. Tomographic inversion of seismic refraction data from the flanks of the East Pacific Rise (EPR), 17°15'S, shows that the thickness of layer 2 varies by as much as 500 meters off axis. A thick layer 2 is found in crust affected by migration paths of overlapping spreading centers (OSC). However, no significant variation in crustal thickness is detected throughout the study area. The crustal structure differences documented in this paper are primarily related to this paleo-tectonic setting rather than the east-west asymmetries characteristic of this region of the southern EPR.

Introduction

The Mantle ELectromagnetics and Tomography (MELT) experiment was designed to provide observations on the distribution of melt and the pattern of mantle upwelling under the southern EPR[*Forsyth et al.*, in press]. The seismic refraction portion of the MELT experiment was conducted in Fall 1995 and consisted of two linear ocean bottom seismometer (OBS) arrays shot with a 4450 cu. in. airgun array from the R/V Melville. The primary array, the topic of this study, crosses the EPR at 17°15'S, and refraction data were collected along two segments (Line 2 and Line 3, Figure 1). The secondary array[*Canales et al.*, in press] crosses the EPR 150 km to the north, near a small OSC.

In this area, the axis of the ultra-fast spreading EPR (142 mm/yr) is shallow (<2600m deep) and displays a broad inflated cross-section. The spreading rate[eg. *Cormier and Macdonald*, 1994], seamount densities and subsidence rates[*Scheirer et al.*, 1996b] and Mantle Bouguer Anomalies (MBA)[*Scheirer et al.*, in press] are all asymmetric about the ridge axis, with the east flank subsiding at the average global rate, having relatively few seamounts and exhibiting horst and graben topography. The west flank subsides at about half the average rate, spreads on average slower than the east flank and is dotted by the abundant seamounts of the Rano Rahi field. Line 3 intersects two major seamounts chains, the Anakena and Patia chains (Figure 1).

[1]LeRoy M. Dorman, Donald W. Forsyth, Jason Phipps-Morgan, Daniel S. Scheirer, Maya Tolstoy and Spahr C. Webb

Paper number 98GL51590.
0094-8534/98/98GL-51590$05.00.

Data analysis

Airgun travel-time data have been analyzed by forward raytracing and 2D-tomographic modeling[*Van Avendonk et al.*, in press]. Our solution to the forward raytracing problem is an adaptation of Moser's shortest path[*Moser*, 1991] and conjugate gradient ray bending algorithms[*Moser et al.*, 1992] which provide sufficiently accurate travel-times and stable raypaths. Rough topography (seamounts and abyssal hills) dictates that we use sheared grid cells, allowing the top of the velocity grid to match the ocean floor[*Toomey et al.*, 1994]. We alternate raytracing with linearized inversions for the P-velocity model. We choose to over-parameterize the model, which allows us to resolve fine-scale variations in the 2D velocity field if required by the data. While performing the tomographic inversion, we minimize an objective function that is a linear combination of the data fit and the velocity model roughness. The roughness penalty is an integral over squared, scaled vertical and horizontal derivatives. The horizontal length scale is constant and up to a few orders of magnitude larger than the vertical one, reflecting the expectation of modest lateral variations. The vertical length scale increases with depth and is based on a reference EPR velocity model [*Vera et al.*, 1990].

A total of 6126 vertical component P-wave arrivals were picked including 3425 clear crustal refractions (Pg), 1651 Moho reflections (PmP) observed on most of our record sections, and 1050 mantle refractions (Pn), mostly on the west flank of the ridge. This allowed us to obtain 2D velocity models (Figure 2A,D) for both flanks of the ridge axis. Typically, the seismic structure of the oceanic crust is described in terms of layers with the boundaries between the layers being marked by changes in velocity gradient. The shallowest layer, layer 2A, is divided from the top of layer 2B, a nearly constant section, by a steep velocity gradient from 2.4 to 5 km/s[eg. *Harding et al.*, 1993]. The transition into layer 3 is generally interpreted to coincide with a decreasing gradient at about 6.6 km/s[eg. *Vera et al.*, 1990]. Our final velocity models are too smooth to use velocity gradients to define the seismic layers and we choose 5 and 6.6 km/s velocity contours as proxies to delimit layer 2A, 2B and 3 (see contours on Figure 2B,E). Ray coverage is much greater in the upper-crust than in the lower crust, allowing greater confidence in the location of the layer 2/3 interface than the Moho depth.

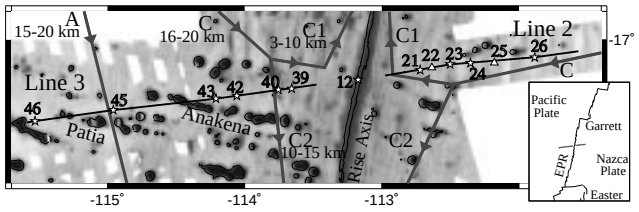

Figure 1. Thin lines are the seismic refraction profiles located on the flanks of the EPR between Garrett Fracture Zone and Easter Microplate. Symbols show the positions of the 13 OBSs. The bathymetry data were primarily collected during the Gloria and Rapa expeditions [*Scheirer et al.*, 1996a]. Superimposed is a sketch highlighting the approximate migration paths (thick arrows) of OSCs constrained by magnetic anomalies and side-scan lineaments by *Cormier et al.* [1996] (approximate offset and nomenclature are indicated).

The Moho reflector is initially placed at 7.5 km/s where the high velocity gradient of the transition zone starts, and is assumed to be flat, an approximation that is justified by the absence of a trend in the PmP travel-time residuals. The average crustal thickness is estimated to be 5.5 km on the Pacific plate and 5.2 km on the Nazca plate, using both Pg-Pn cross-over ranges and PmP travel-times. These estimates are in good agreement with thickness bounds independently obtained by *Canales et al.* [in press] - 4.8 to 5.6 km on the Pacific plate and 5.1 to 5.7 km on the Nazca plate. The computed vertical incidence reflection times of the Moho are 1.75 sec on the Pacific plate and 1.71 sec on the Nazca plate. These predictions are consistent with actual Moho reflection times of 1.7 sec on both flanks in a multi-channel seismic profile crossing the EPR at 17°34'S [*J. M. Babcock*, pers. comm.], providing confirmation that the crustal thicknesses are accurate and similar on both sides of the ridge.

Observations

On the west flank (Line 3, Figure 2A) there are two interesting features in our crustal velocity model. First, we observe a thickening of all upper crustal layers in the vicinity of the two main chains of seamounts. Second, layer 2 (2A + 2B) is 1.5-1.6 km thick away from the influence of the seamount chains, with the exception of a short ∼15 km section west of OBS 40 (Figure 2A,B) where the thickness is 2.0-2.1 km. This step in thickness is required by the data and the good ray coverage gives us confidence in defining this feature. This step coincides with the presence at the ridge 0.78 Ma ago of a paleo-overlapping spreading center denoted "C2" (see Figure 1 and[*Cormier et al.*, 1996]). A similar feature may be expected where the wake of OSC "A" intersects Line 3 at right angles near OBS 45, but the original structure is overprinted by seamount magmatism and in any case ray coverage and hence resolution are poor in this area.

The crustal structure on the east flank (Line 2, Figure 2D) is quite different from that found on the west flank with an almost uniform layer 2 thickness (2.0-2.1 km). The position of Line 2 is very close to the center of the Nazca plate track of the large OSC "C" that migrated south along the EPR from 3 Ma to 1 Ma and subsequently bifurcated at 1 Ma, into two smaller OSCs "C1" and "C2" which rapidly migrated away from each other (Figure 1 and[*Cormier et al.*, 1996]). We observe a thinning of layer 2 60 km off axis (1.5-1.6 km thick below OBSs 22 and 23, Figure 2D,E); at this range the crust is no longer affected by the ∼40 km wide corridor that constitutes the discordant zone of OSC "C". The narrow ∼20 km wide corridor formed by the smaller OSC "C1" starts to affect Line 2 (west of OBS 22) as it approaches its western end.

Velocity models and OSC migration patterns (see green colored bands delineating the areas affected by OSC paths on Figure 2A,D) suggest that there is a correlation between layer 2 thickness and the presence of OSCs. In crust not affected by seamount magmatism, layer 2 is ∼500 m thicker when it lies within the corridor of an OSC migration path.

The two main features of our interpretation - layer 2 thickening west of OBS 40 and thinning below OBSs 22 and 23 - have a gravity signature compatible with the data. We used the ship gravity data (Figure 3 in dark) as an independent check on the two key seismic observations. We modeled the residual Bouguer Anomaly (Figure 3 in light) using the three crustal layers (Figure 2B,E) derived from our 2D seismic models. The short wavelength features in the residual BA are expected to reflect variations in crustal densities and thicknesses. On both flanks, the modeled amplitudes fit the gravity data reasonably well. The mismatch between data and predictions at the center of the west line, is due to the effect of the large seamounts south of OBSs 43 and 45. Their loading effect modifies the density distribution in 3D while our seismic tomography resolves only the 2D structure.

Discussion and conclusions

The distinct crustal structures found along the west and east profiles probably do not reflect a typical asymmetry about the southern EPR. Because the profiles are oblique to the ridge axis, the west-flank crust was created mainly at the center of a second-order ridge segment, segment "G" and the east-flank crust was created at the end of a segment, segment "L" (nomenclature as in[*Hooft et al.*, 1997]). The profiles instead provide us with an opportunity to examine crustal structure associated with OSCs and OSC wakes, features for which there are, as yet, very few direct seismic measurements. The most notable features of the seismic models is the increase in layer 2 thickness in the OSC wakes and the absence of any change in crustal thickness.

Although morphologically OSCs form segment boundaries and are frequently assumed to be located away from focused mantle upwelling[*Macdonald et al.*, 1988], there is not a consensus as to whether this should mean thinner or thicker crust at OSC. Seismic data indicate thick crust immediately north of the 9°03'N OSC [*Barth and Mutter*, 1996; *G. M. Kent* pers. comm. from ARAD 3D preliminary results], while gravity data have been interpreted as indicating thick crust at the 22°10'S OSC along the Valu Fa ridge[*Sinha*, 1995]. Conversely a positive residual MBA in the vicinity of 20°40'S OSC along the EPR has been interpreted as due to a crustal thinning of 500±200m[*Cormier et al.*, 1995]. Our observations suggest that the crustal thickness remained constant and normal throughout the propagations of paleo-ridge segments in the MELT area.

The most straightforward explanation of the seismic layer 2/3 boundary is as a porosity horizon, one whose relation-

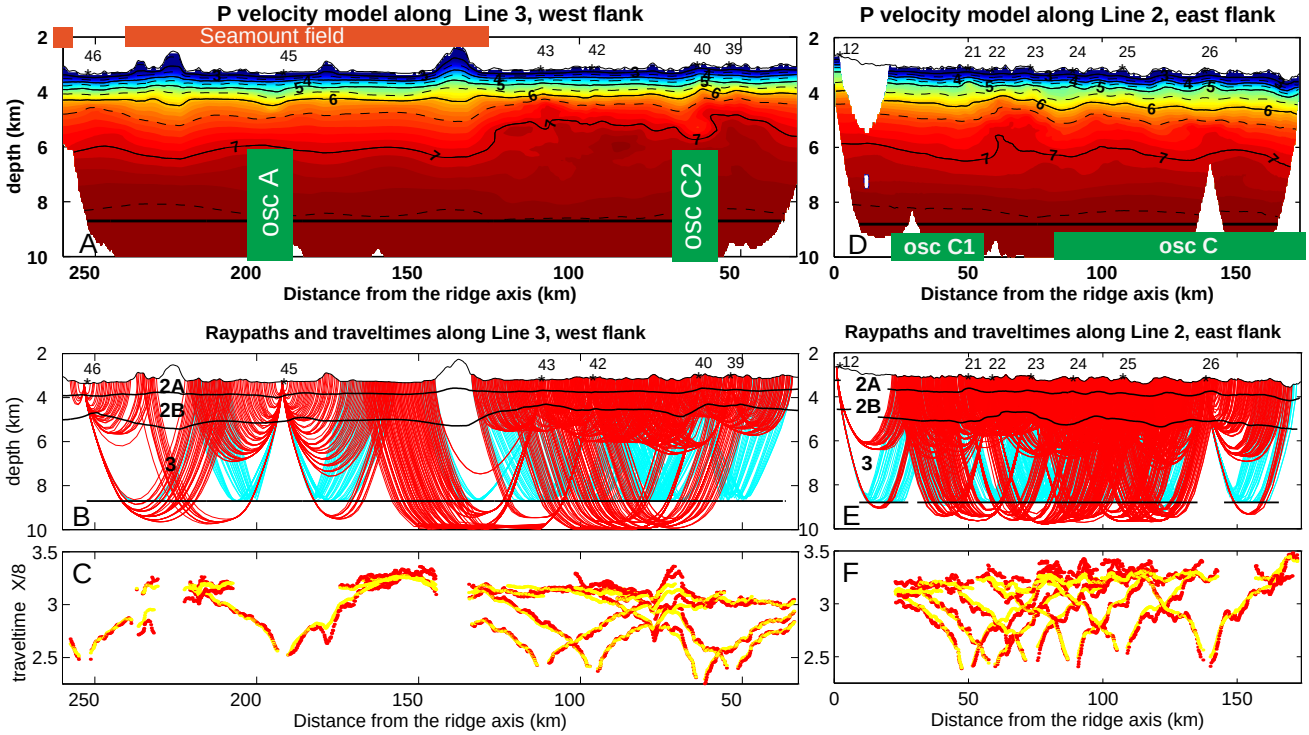

Figure 2. The color panels (A,D) show the 2D velocity models. The solid and dashed lines are velocity contours. The red colored bands show the extent of the seamount field and the green ones the areas affected by OSC paths. The top panels (B,E) display the position of the OBSs along the lines and every other raypaths. The light rays are PmP that reflect from a flat reflector representing the Moho and the dark rays are the Pg and Pn. The interfaces between the layers 2A, 2B and 3 are highlighted. The lower panels (C,F) are reduced travel-times plots of the data picks (dark) and calculated travel-times (light). The χ^2 reduces from 20 before inversion to 1.7 after inversion on the west line (the median of the travel-time residuals is 19 msec after inversion), and from 11 to 5 on the east line (the median is 35 msec). The general fit of the travel-time data for Line 2 is not as good as for Line 3 because of the rougher seafloor fabric within the OSC wakes.

ship to the underlying lithologic layering need not be fixed. For the magmatically dominated segments of the EPR, the depth of layer 2/3 boundary is observed to be at or near the depth the axial magma chamber (AMC) reflector, after making allowance for the off-axis thickening of layer 2A[eg. *Vera et al.*, 1990]. Such a relationship can arise if, for example, the cracking front due to the hydrothermal circulation is buffered by, and lies just above the AMC. In these circumstances the off-axis layer 2/3 boundary will track the fossil depth of the magma sill roof averaged over times of a few hundred thousand years and a more magmatically robust segment with a shallower average AMC depth would produce a thinner layer 2. These observations need not apply to the more tectonically active OSC basins [*Macdonald et al.*, 1988; *Wilcock et al.*, 1992] where fracturing of the upper crust may be the dominant influence on the layer 2/3 boundary. *Christeson et al.* [1997] detected lower layer 2 velocities and perhaps a thicker layer 2 in crust affected by the 9°03'N OSC wakes, which they attribute to an increase of upper crustal porosity caused by shearing and rotation of the overlap basins. However, the depth of the layer 2/3 transition in our velocity models - 1.5 to 1.6 km for crust created at the center of the segment, and 2.0 to 2.1 km for crust created near an OSC - is what one would predict for the fossil depth from present day variations in AMC depth along the southern EPR. AMC depths occur typically ∼500 m shallower at the center of segment than at OSCs, deepening from ∼1.2 to 1.7 km[*Hooft et al.*, 1997], and the off-axis increase in layer 2A thickness is typically ∼300-400 m[eg. *Harding et al.*, 1993]. This coincidence in depth may be fortuitous given the inherent vertical resolution of our tomographic models, and more detailed geophysical studies will be required to resolve this question. However, it is conceivable that the enhanced tectonism of the OSC could be the proximal cause of a deeper layer 2/3 transition and a deeper AMC. One hypothesis is that the magma sill resides at a freezing surface controlled by a balance between heat input by injection of magma into the crust and heat removal by hydrothermal circulation[eg. *Henstock et al.*, 1993; *Phipps-Morgan and Chen*, 1993]. Enhanced cooling linked to the particular geometry of the ridge at an OSC would in this case explain the deepening of the magma sill and the absence of concomitant reduction in crustal thickness.

In addition, our results indicate that the east-west asymmetry of the MBA across the EPR in the MELT area [*Scheirer et al.*, in press] cannot be explained by a difference in crustal thickness and is probably created by asymmetric upper mantle temperatures. Seismological observations[*Forsyth et al.*, in press] demonstrate that lower mantle velocities and stronger anisotropy are present on the west side of the rise axis, suggesting that the melt production is shifted toward the Pacific plate in this area. Our observations of clearer and stronger Pn arrivals on the west side of the EPR suggest that a high temperature, high melt anomaly cannot reside in the upper 2-3 km of the mantle. However, high anisotropy in the uppermost mantle due to

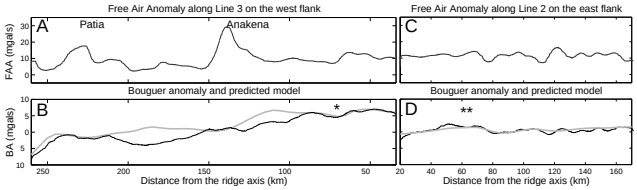

Figure 3. The observed Free Air gravity anomalies (A,C) are mainly due to the Anakena and Patia seamount chains on the west flank and to the abyssal hills on the east flank. The residual Bouguer Anomaly is obtained by subtracting from the FAA the predicted gravity signature of a constant density (2.7 g/cm^3) half space with the bathymetry grid, and a linear regional trend (5.5 mgals/Ma for the Pacific plate and 12.5 mgals/Ma for the Nazca plate estimated from the regional MBA profiles [*D. S. Scheirer*, pers. comm.] for a crust between 1 Ma and 5 Ma). Variations in the residual BA (B,D, in dark) are on the order of 10 mgals for the west flank and 5 mgals for the east flank, confirming that the east line exhibits minor lateral variations in structure. We model the BA directly (B,D, in light) using three layers of constant density (2.7 g/cm^3 for layer 2A, 2.85 g/cm^3 for layer 2B and 2.95 g/cm^3 for layer 3, [*Carlson and Raskin*, 1984]) derived from our 2D seismic models. The volcanic layer thickening west of OBS 40 (marked by $*$ on B) and thinning below OBSs 22 and 23 ($**$ on D) have a gravity signature compatible with the data.

the shearing of faster Pacific plate motion relative to the deep mantle, as suggested by *Forsyth et al.* [in press], could be responsible for our observations.

Acknowledgments. This work has been supported by NSF grant OSE9406146. We thank V. Ballu for her aid with the gravity data and M. H. Cormier, J. M. Babcock and D. K. Blackman for helpful discussions.

References

Barth, G. A. and J. C. Mutter, Variability in oceanic crustal thickness and structure: multichannel seismic reflection results from the northern East Pacific Rise, *J. Geophys. Res., 101,* 17,951-17,975, 1996.

Canales, J. P., R. S. Detrick, S. Bazin, A. J. Harding and J. A. Orcutt, Off-axis crustal thickness variations across and along the East Pacific Rise within the MELT area, *Science*, in press, 1998.

Carlson, R. L. and G. S. Raskin, Density of oceanic crust, *Nature, 311*, 555-558, 1984.

Christeson G. L., P. R. Shaw and J. D. Garmany, Shear and compressional wave structure of the East Pacific Rise, 9°-10°N, *J. Geophys. Res., 102,* 7821-7835, 1997.

Cormier, M. H. and K. C. Macdonald, East Pacific Rise 18°-19°S: asymmetric spreading and ridge reorientation by ultrafast migration of axial discontinuities, *J. Geophys. Res., 99,* 543-564, 1994.

Cormier, M. H., K. C. Macdonald and D. S. Wilson, A three-dimensional gravity analysis of the East Pacific Rise from 18° to 21°30'S, *J. Geophys. Res., 100,* 8063-8082, 1995.

Cormier, M. H., D. S. Scheirer and K. C. Macdonald, Evolution of the East Pacific Rise at 16°-19°S since 5 Ma: bisection of overlapping spreading centers by new, rapidly propagating ridge segments, *Mar. Geophys. Res., 18,* 53-84, 1996.

Forsyth, D. W. and the MELT Seismic Team, Imaging the deep structure beneath a mid-ocean ridge: overview of the seismological component of the MELT experiment, *Science*, in press, 1998.

Harding, A. J., G. M. Kent and J. A. Orcutt, A multichannel seismic investigation of upper crustal structure at 9°N on the East Pacific Rise: implications for crustal accretion, *J. Geophys. Res., 98,* 13,925-13,944, 1993.

Henstock, T. J., A. W. Woods and R. S. White, The accretion of oceanic crust by episodic sill intrusion, *J. Geophys. Res., 98,* 4143-4161, 1993.

Hooft, E. E. E., R. S. Detrick and G. M. Kent, Seismic structure and indicators of magma budget along the Southern East Pacific Rise, *J. Geophys. Res., 102,* 27,319-27,340, 1997.

Macdonald, K. C., R. M. Haymon, S. P. Miller, J.-C. Sempere and P. J. Fox, A new view of the mid-ocean ridge from the behavior of ridge-axis discontinuities, *J. Geophys. Res., 93,* 2875-2898, 1988.

Moser, T. J., Shortest path calculation of rays, *Geophysics, 56*, 59-67, 1991.

Moser, T. J., G. Nolet and R. Snieder, Ray bending revisited, *Bull. Seismol. Soc. Am., 82,* 259-288, 1992.

Phipps-Morgan, J. and Y. J. Chen, Dependence of ridge-axis morphology on magma supply and spreading rate, *Nature, 364*, 706-708, 1993.

Scheirer, D. S., K. C. Macdonald, D. W. Forsyth, S. P. Miller, D. J. Wright, M. H. Cormier and C. M. Weiland, A map series of the southern East Pacific Rise and its flanks, 15°S to 19°S, *Mar. Geophys. Res., 18,* 1-12, 1996a.

Scheirer, D. S., K. C. Macdonald, D. W. Forsyth and Y. Shen, Abundant seamounts of the Rano Rahi seamount field near the Southern East Pacific Rise, 15°S to 19°S, *Mar. Geophys. Res., 18,* 13-52, 1996b.

Scheirer, D. S, D. W. Forsyth, M. H. Cormier and K. C. Macdonald, Shipboard geophysical indications of asymmetry and melt production beneath the East Pacific Rise near the MELT experiment, *Science*, in press, 1998.

Sinha, M. C., Segmentation and rift propagation at the Valu Fa ridge, Lau Basin: evidence from gravity data, *J. Geophys. Res., 100,* 15,025-15,043, 1995.

Toomey, D. S., S. C. Solomon and G. M. Purdy, Tomographic imaging of the shallow crustal structure at 9°30'N, *J. Geophys. Res., 99,* 24,135-24,157, 1994.

Van Avendonk, H. J. A., A. J. Harding, J. A. Orcutt and McClain J. S., A 2-D tomographic study of the Clipperton transform fault, *J. Geophys. Res.,* in press, 1998.

Vera, E. E., J. C. Mutter, P. Buhl, J. A. Orcutt, A. J. Harding, M. E. Kappus, R. S. Detrick and T. M. Brocher, The structure of 0- to 0.2m.y.-old oceanic crust at 9°N on the East Pacific Rise from expanded spread profiles, *J. Geophys. Res., 95,* 15,529-15,556, 1990.

Wilcock, W. S. D., G. M. Purdy, S. C. Solomon, D. L. DuBois and D. S. Toomey, Microearthquakes on and near the East Pacific Rise, 9°-10°N, *Geophys. Res. Lett., 19,* 2131-2134, 1992.

Sara Bazin, IGPP, Scripps Institution of Oceanography, UCSD, La Jolla, CA 92037-0225. (e-mail: sbazin@ucsd.edu)

(Received December 9, 1997; revised March 5, 1998; accepted April 30, 1998.)